Structural Engineering and Mechanics, Vol. 12, No. 4 (2001) 377-396
DOI: http://dx.doi.org/10.12989/sem.2001.12.4.377

Application of a 3-D crack analysis model to RC cantilever decks of excessive cracking

Zihai Shi† and Masaaki Nakano‡

Research and Development Center, Nippon Koei Co., Ltd., 2304 Inarihara, Kukizaki-machi, Inashiki-gun, Ibaraki 300-1259, Japan

Abstract. The excessive cracking of RC cantilever decks, which often requires special attention for structural engineers, is studied using a three-dimensional crack analysis model. The model is based on a fracture energy approach for analyzing cracks in concrete, and the numerical analysis is carried out using a modified load control method. The problem of excessive cracking is then studied with four different span-ratios. Based on the numerical results, the crack behavior with respect to the patterns of crack propagation, dissipation of the fracture energy, and effects on the structural integrity are discussed. The mechanisms which cause the excessive cracking are also explained.

Key words: RC cantilever decks; 3-D crack analysis; fracture energy; load control.

1. Introduction

As shown in Fig. 1, single-column supported reinforced concrete (RC) cantilever decks are widely used in elevated highway systems. Since the deck surface is under constant tension, the cracking behavior and crack control are of great concern for structural engineers. Illustrated also in Fig. 1 is an example of excessive cracking on the deck surface which is quite typical of this type of structure. Although most building code requirements for structural concrete should lead to adequate crack control, the provisions typically focus on reinforcement details rather than on crack behavior. Therefore, the crack control is sometimes not sufficient under complicated stress states. As such,

Fig. 1 Single-column supported RC cantilever decks and excessive cracking on the surface

† Senior Researcher
‡ Researcher

special investigation on crack behavior and precautions for crack control are required in certain situations.

It is known that excessive cracking must be avoided not only for aesthetic reasons, but also because damage to the protection of reinforcement against corrosion greatly affects any structure's safety. Obviously, the excessive cracking of RC cantilever decks depends very much on the span-ratio (the ratio of the longer span to the shorter span) as well as on the reinforcement details. Because of the complicated stress states in cantilever decks, a three-dimensional crack analysis model for RC cantilever decks has been proposed (Shi and Nakano 1999).

In Sections 2 to 4, the theoretical aspects of the model are explained in detail. These include a modified load control method which enables the non-linear response with limit points to be analyzed using only the load control methods. Next, a fracture energy approach to the crack analysis of concrete is explained. It consists of an energy criterion for determining the equivalent length, and an analysis method based on variations of the fracture energy and the strain energy. Based on this energy approach, a three-dimensional crack analysis model is established. In order to facilitate convergence of the numerical solutions, the E'-ω relation is used directly in the total formulation of the constitutive relation for the fractured elements. A numerical algorithm enabling the incremental elasto-plastic analysis of concrete to be carried out simultaneously with the crack analysis, is also explained.

In Section 5, the model is applied to the problem of excessive cracking of RC cantilever decks, with four different span-ratios. Based on the numerical results, crack behavior with respect to the patterns of crack propagation, dissipation of the fracture energy, and the effects on the structural integrity are discussed. The mechanisms which cause the excessive cracking are also analyzed.

2. A modified load control method

In the crack analysis of concrete, limit points (maximum loads) are often the cause of concern before choosing a numerical approach to analyze the problem. Although the traditional load control method is most suitable in many engineering applications, numerical iterations diverge as the load level approaches these limit points. Theoretically, other approaches such as the displacement control method and the arc-length control method overcome the problem. For systems with many degrees of freedom, however, these procedures are harder to implement than in the case of simple problems with few degrees of freedom. Taking the fracture tests of plain concrete beams as an example, numerical analyses using the displacement control method may fail even in these simple situations, due to the snap-back phenomenon. In the following, a modified load control method is introduced to overcome these difficulties while retaining the fundamental characteristics of a traditional load control procedure by calculating displacements for loads, except that numerical iterations are carried out at a load level that is not fixed.

The standard equilibrium equation for proportional loading is expressed as

$$\lambda P - F(x) = 0 \tag{1}$$

where P is a vector of reference loads, λ is the proportional loading factor, F is a vector of the internal forces, and x is the total displacement. This is traditionally solved using a Newton incremental iterative solution:

Fig. 2 A modified load control method

$$K^{(i)}\Delta u = \lambda P - F(x^{(i)}) \tag{2}$$

$$x^{(i+1)} = x^{(i)} + \Delta u. \tag{3}$$

where $K^{(i)}$ is the tangent stiffness matrix, Δu is the incremental displacement, and the superscripts in the parentheses denote the number of approximation to the true solution.

In the modified load control method, instead of computing the displacement at a fixed load level through iterative procedures of Eqs. (2) and (3), the displacement at a lower load level is calculated through a guided load-reducing procedure. As shown in Fig. 2, the initial displacement increment $\Delta u^{(1)}$ for the initial load increment $\Delta\lambda^{(1)}P$ is

$$\Delta u^{(1)} = [K^I]^{-1}\Delta\lambda^{(1)}P. \tag{4}$$

where K^I is the tangent stiffness at the beginning of the iterations, which is used to evaluate the initial displacement increment $\Delta u^{(1)}$. Note that in Fig. 2, the left superscript m indicates the current configuration of the total displacement ${}^m x$, and the load ${}^m P = {}^m\lambda P$. The residual force $R^{(1)}$, which is also used conveniently here as an amount of load reduction, is then given by

$$R^{(1)} = \Delta\lambda^{(2)}P = \left({}^m\lambda + \Delta\lambda^{(1)}\right)P - F\left({}^m x + \Delta u^{(1)}\right). \tag{5}$$

At a prescribed value of the stiffness parameter K^{II} ($K^{II} > K^I$), the displacement decrement $\Delta u^{(2)}$ is

$$\Delta u^{(2)} = [K^{II}]^{-1}\Delta\lambda^{(2)}P. \tag{6}$$

A new iteration point (point 2) is then obtained by subtracting the current load and displacement by the amount of $\Delta\lambda^{(2)}P$ and $\Delta u^{(2)}$ respectively, as

$$\lambda^{(2)}P = \left({}^m\lambda + \Delta\lambda^{(1)} - \Delta\lambda^{(2)}\right)P \tag{7}$$

$$x^{(2)} = {}^m x + \Delta u^{(1)} - \Delta u^{(2)}. \tag{8}$$

A general formulation is given by

$$R^{(i)} = \Delta\lambda^{(i+1)}P = \left({}^m\lambda + \Delta\lambda^{(1)} - \sum_{k=2}^{i}\Delta\lambda^{(k)}\right)P - F\left({}^m x + \Delta u^{(1)} - \sum_{k=2}^{i}\Delta u^{(k)}\right) \tag{9}$$

$$\Delta u^{(i+1)} = [K^{II}]^{-1} \Delta\lambda^{(i+1)} P \tag{10}$$

$$\lambda^{(i+1)} P = \left({}^{m}\lambda + \Delta\lambda^{(1)} - \sum_{k=2}^{i+1} \Delta\lambda^{(k)} \right) P \tag{11}$$

$$x^{(i+1)} = {}^{m}x + \Delta u^{(1)} - \sum_{k=2}^{i+1} \Delta u^{(k)} \tag{12}$$

where i=2, 3…. The above iterative procedures are repeated to eliminate the residual forces until the desired accuracy is achieved at $i=n$. Finally, the new equilibrium position m+1 is given by

$${}^{m+1}\lambda P = \left({}^{m}\lambda + \Delta\lambda^{(1)} - \sum_{k=2}^{n} \Delta\lambda^{(k)} \right) P \tag{13}$$

$${}^{m+1}x = {}^{m}x + \Delta u^{(1)} - \sum_{k=2}^{n} \Delta u^{(k)}. \tag{14}$$

Although the residual forces are used as the load reductions in the above formulations, this is only a matter of convenience. In fact, with small load decrements properly chosen for iterations the new equilibrium position m+1 could also be reached. As explained later, the modified load control method described above varies slightly in the crack analysis of concrete, due to the characteristics of the numerical approach employed, as well as the nature of the problem.

3. Fracture energy approach

3.1 An energy criterion and equivalent length

The energy approach stipulates that a crack propagates when the energy available for crack growth is sufficient to overcome the resistance of the material. The energy principle is often expressed in terms of the energy release rate g, which is defined as the rate of change in potential energy with crack area for a linear elastic material. When $g = g_c$ with g_c being the critical energy release rate, either a new crack initiates or an existing crack extends.

In concrete the crack growth resistance results from the development of the fracture process zone and the bridging of the crack by aggregate, and is governed by the tensile softening law. Therefore, as a crack extends, the rate of energy dissipation with crack area g_f' can be calculated from the tensile softening curve. Obviously, the energy dissipated in the process of cracking is the amount of energy required for creating the same crack, excluding the energy dissipation due to plasticity outside the crack. Thus, similar to the energy release rate, it seems reasonable to assume $g_f' = g_{fc}'$ with g_{fc}' being the material's resistance to fracture at the moment of cracking.

In Fig. 3, a linear stress-displacement relation for the FPZ expressed in the stress-strain form is assumed for simplicity. Based on the smeared crack approach, a crack is smeared along an equivalent length l, which is the length of the fractured domain perpendicular to the crack (Dahlblom and Ottosen 1990). Suppose that at a certain load level crack propagation starts from a point A and stops at a point B, while the cohesive stress σ drops from f_t' (= βf_t) to f_t'' (= γf_t).

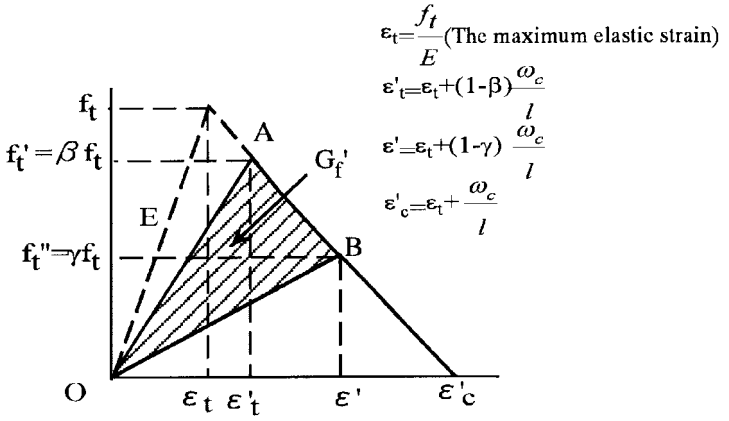

Fig. 3 Energy dissipation due to cracking

Here, f_t is the material's original tensile strength and $0 \le \gamma < \beta \le 1$. In the following, the equivalent length l is derived from the rate of energy dissipation g_f' and the material's resistance to fracture g_{fc}'. From Fig. 3, the dissipated energy G_f' is given by

$$G_f' = \Delta OAB = \frac{1}{2}(\beta - \gamma) f_t \varepsilon_c'. \tag{15}$$

Analogous to the definition of the energy release rate, the rate of energy dissipation g_f' is defined as

$$g_f' = \frac{G_f'}{\Delta\omega} = \frac{\Delta OAB}{(\beta-\gamma)\omega_c} = \frac{f_t \varepsilon_c'}{2\omega_c} = \frac{f_t}{2}\left(\frac{f_t}{\omega_c E} + \frac{1}{l}\right) \tag{16}$$

where $\Delta\omega$ is the incremental crack opening displacement, ω_c is the limiting crack opening displacement, ε_c' is the limiting fracturing strain, and E is Young's modulus. Solving Eq. (16) for l with $g_f' = g_{fc}'$ leads to

$$l = \frac{1}{\dfrac{2g_{fc}'}{f_t} - \dfrac{f_t}{\omega_c E}}. \tag{17}$$

Eq. (17) shows that the equivalent length l, which depends on the material's resistance to fracture g_{fc}' as well as the material properties f_t, E and ω_c, is a constant as long as a linear softening law is assumed. In this study, g_{fc}' is calculated from the initial crack using Eq. (16), and the equivalent length l is taken as the length of the maximum projection of the mesh normal to the direction of the initial crack. Hence, g_{fc}' serves as an index to reflect both the material resistance and the mesh characteristics against cracking. After the initial cracking, the equivalent length of subsequent cracks is computed from Eq. (17). When a bi-linear softening law is adopted, the equivalent length l is no longer a constant; it varies as the crack growth crosses the concave point formed by the two straight lines. Derivation of the equivalent length l for a bi-linear softening law is omitted here.

3.2 Fracture energy dissipation and strain energy loss

As cracks propagate in concrete, the dissipation of fracture energy at cracks leads to the loss of

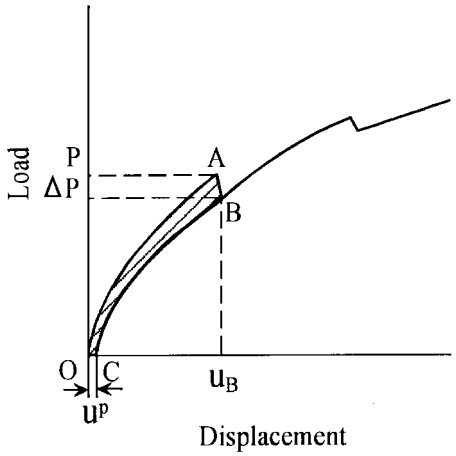

Fig. 4 Loss of strain energy due to cracking

strain energy in the structure. According to the principle of energy conservation, the amount of strain energy loss in the system equals the amount of fracture energy dissipation. Here, consider only a single concentrated load acting on a concrete structure. On the load-deflection curve in Fig. 4, the shaded area *OABC* represents the total strain energy loss ΔU_f after stable cracks occur or extend at the load level *P*, and is approximately obtained as

$$\Delta U_f = \frac{1}{2}(u_B - u^P)\Delta P. \tag{18}$$

Here, u^p is the residual displacement due to plasticity, and ΔP is the total load reduction after cracking. Although the residual part u^p may become significant in the post-peak region as structural failure progresses, it is generally ignorable when compared with the total displacement u_B up to the maximum load. For simplicity, this term is omitted in the following numerical studies, because the cracking behavior of RC cantilever decks to be studied is apparently confined to the pre-peak region. The total dissipation of fracture energy ΔW_f is obtained by integrating G_f' of Eq. (15) over the entire fractured area V_c as

$$\Delta W_f = \int_{V_c} G_f' dV = \sum_{\alpha=1}^{N} G_f'^{\alpha} V^{\alpha} \quad \text{with} \quad \sum_{\alpha=1}^{N} V^{\alpha} = V_c. \tag{19}$$

Here, V^{α} is the area of the element where crack α occurs, and N is the total number of cracks. Equalizing the strain energy loss ΔU_f with the dissipation of fracture energy ΔW_f leads to

$$\Delta U_f = \Delta W_f . \tag{20}$$

Numerically, the new equilibrium position *B* in Fig. 4 is obtained by computing Eq. (18) for a number of small negative load increments until the total strain energy loss ΔU_f satisfies Eq. (20). Then, summing up these small load decrements yields the total load reduction ΔP. When used with the modified load control method, these small negative load increments replace the residual forces as the load reductions in the guided load reduction procedure, and Eq. (20) serves as the criterion to terminate this process.

4. Three-dimensional crack modeling

4.1 Basic assumptions on cracks

The following assumptions are imposed upon the three-dimensional crack modeling for RC cantilever decks. A crack is restricted to occur only as either an in-plane crack (the crack plane is perpendicular to the deck plane) or an out-of-plane crack (the crack plane is parallel to the deck plane). In other words, one of the three principal stresses at any stress point is supposed to coincide with the direction normal to the deck plane. Furthermore, the two in-plane cracks are restricted to occur only in the directions perpendicular to each other. Once occurred, crack orientations are then fixed. As a matter of fact, these restrictions on cracks fall into the category of the so-called multidirectional-fixed crack approach. This is considered to be a reasonable approximation to the actual stress states in RC cantilever decks, considering the small thickness of the decks when compared with the other two dimensions.

Although somewhat poor accuracy in the resulting solutions could be anticipated, it is compensated not only by a simpler formulation of the problem but also by a clearer picture on cracks.

4.2 The smeared constitutive relation based on the E′-ω relation

To ensure that the loss of concrete rigidity in the fractured elements is irreversible as cracks extend, and thus leading to an easy convergence of the numerical solutions, the constitutive relation for these elements is formulated directly using the E'-ω relation. Here, ω is the crack-opening width, and E' is the apparent elasticity and defined as

$$E' = \frac{\sigma}{\varepsilon'} = \frac{\sigma}{\varepsilon_t + \omega/l} = \frac{\sigma}{f_t/E + \omega/l} \tag{21}$$

where ε' is the fracturing strain, ε_t is the maximum elastic strain, and σ is the cohesive stress defined by the tensile softening law. The equivalent length l provides a measure of the region over which the crack opening width ω is smeared to establish the fracturing strain. A series of deformation-controlled uni-axial tensile tests on narrow concrete specimens had been carried out to obtain the relation between the apparent elasticity E' and the crack opening width ω. In the following numerical applications, a bi-linear approximation to the actual E'-ω relation shown in Fig. 5 is employed. In the same figure, a bi-linear approximation to the tensile softening law of concrete is also given, and these two relations form the bases for the crack analysis.

The general constitutive relation expressing strains in terms of stresses is

$$\begin{Bmatrix} \varepsilon_{1'1'} \\ \varepsilon_{2'2'} \\ \varepsilon_{3'3'} \\ \varepsilon_{1'2'} \\ \varepsilon_{2'3'} \\ \varepsilon_{3'1'} \end{Bmatrix} = \begin{bmatrix} 1/E_{1'} & -\nu_{2'1'}/E_{2'} & -\nu_{3'1'}/E_{3'} & 0 & 0 & 0 \\ -\nu_{1'2'}/E_{1'} & 1/E_{2'} & -\nu_{3'2'}/E_{3'} & 0 & 0 & 0 \\ -\nu_{1'3'}/E_{1'} & -\nu_{2'3'}/E_{2'} & 1/E_{3'} & 0 & 0 & 0 \\ 0 & 0 & 0 & 1/G_{2'3'} & 0 & 0 \\ 0 & 0 & 0 & 0 & 1/G_{3'1'} & 0 \\ 0 & 0 & 0 & 0 & 0 & 1/G_{1'2'} \end{bmatrix} \begin{Bmatrix} \sigma_{1'1'} \\ \sigma_{2'2'} \\ \sigma_{3'3'} \\ \sigma_{1'2'} \\ \sigma_{2'3'} \\ \sigma_{3'1'} \end{Bmatrix} \tag{22}$$

where $E_{1'}$, $E_{2'}$ and $E_{3'}$ are the elastic moduli in the $x_{1'}$, $x_{2'}$ and $x_{3'}$ directions, respectively. $\nu_{i'j'}$ is

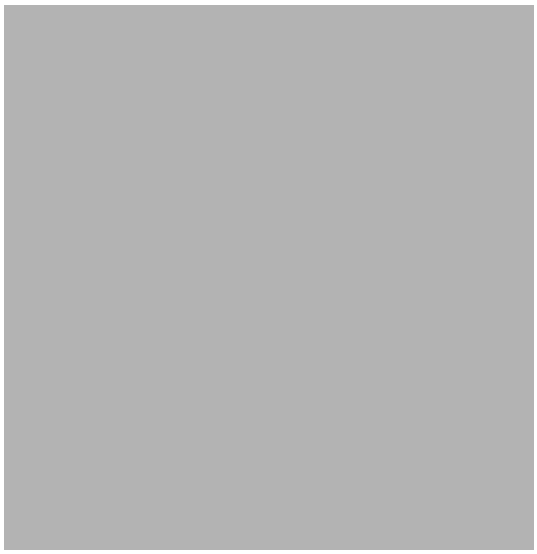

Fig. 5 The E'-ω relation and the tensile softening relation

Poisson's ratio of transverse strain in the $x_{j'}$-direction when stressed in the $x_{i'}$-direction. $G_{2'3'}$, $G_{3'1'}$, $G_{1'2'}$ are shear moduli in the $x_{2'}-x_{3'}$, $x_{3'}-x_{1'}$, and $x_{1'}-x_{2'}$ planes, respectively. The reciprocal relations that must be satisfied in an orthotropic material are omitted here; for more details see Jones (1975). The global stress is then obtained by the following transformation:

$$\begin{Bmatrix} \sigma_{11} \\ \sigma_{22} \\ \sigma_{33} \\ \sigma_{12} \\ \sigma_{23} \\ \sigma_{31} \end{Bmatrix} = \begin{bmatrix} \cos^2\alpha & \sin^2\alpha & 0 & -\sin 2\alpha & 0 & 0 \\ \sin^2\alpha & \cos^2\alpha & 0 & \sin 2\alpha & 0 & 0 \\ 0 & 0 & 1 & 0 & 0 & 0 \\ \frac{1}{2}\sin 2\alpha & -\frac{1}{2}\sin 2\alpha & 0 & \cos 2\alpha & 0 & 0 \\ 0 & 0 & 0 & 0 & \cos\alpha & \sin\alpha \\ 0 & 0 & 0 & 0 & -\sin\alpha & \cos\alpha \end{bmatrix} \begin{Bmatrix} \sigma_{1'1'} \\ \sigma_{2'2'} \\ \sigma_{3'3'} \\ \sigma_{1'2'} \\ \sigma_{2'3'} \\ \sigma_{3'1'} \end{Bmatrix} \tag{23}$$

After a crack develops, the corresponding elastic modulus in Eq. (22) is then replaced by an apparent elasticity E' determined from the E'-ω relation. Fig. 6 sums up the main steps of the crack analysis at an arbitary stress point α (in the three principal stress directions respectively). Note that $f'_{t\alpha}$ is a transient tensile strength after cracking. Obviously, for a perfect element without cracks $f'_{t\alpha}=f_t$. When a crack extends, the crack opening width ω is computed from the fracturing strain ε' and the equivalent length l as

$$\omega = (\varepsilon' - \varepsilon_t)l = \left(\varepsilon' - \frac{f_t}{E}\right)l. \tag{24}$$

Then based on ω the decreasing elasticity E' and cohesive stress σ are obtained from the respective bi-linear relations shown in Fig. 5. If no crack occurs or an existing crack closes, the value of the previous E' is then kept unchanged. In the case of crack closure, it is assumed that the elastic modulus for compression is unaffected by any previous cracks.

Fig. 6 Flow for crack analysis

As for the fracturing strain ε', it is obtained from the incremental elasto-plastic analysis of the structure, by incorporating the constitutive relation of Eq. (22) for the fractured elements into the elasticity matrix of the structure. However, this approach raises a serious question. In order to carry out the crack analysis, the total formulation of the constitutive relation based on the E'-ω relation has to be solved for a total load. On the other hand, the classical theory of plasticity requires an elasto-plastic response of a material to be evaluated step by step by applying the load incrementally, based on an incremental constitutive relation between stress and strain. To employ these two completely different theories (namely, the total strain theory and the incremental strain theory) in a single numerical routine requires a special solution scheme. To that end, a numerical algorithm is proposed and utilized in the numerical solutions to meet the fundamental requirements of the two analyses simultaneously. This solution strategy will be explained later.

4.3 Basic assumptions for elasto-plastic analyses of concrete and reinforcing steel

As stated before, the elasto-plastic behavior of concrete is analyzed using the classical theory of plasticity, and the Drucker-Prager yield criterion is adopted. The uni-axial stress-strain relation of concrete in compression proposed by the Design Standard for Concrete of JSCE is employed, and is shown in Fig. 7. The incremental elasto-plastic stress-strain relation is then built upon the work hardening rule and the normality rule, which postulate the direction of plastic flow.

Reinforcing steel is treated as a one-dimensional element, neglecting its shear stiffness. The stress-strain curve of reinforcing steel is assumed to be perfectly elasto-plastic under both tension and compression, and the bond between steel and concrete is assumed to be rigid.

4.4 Solution structure for the non-linear analysis of concrete

Fig. 8 shows the solution structure for the non-linear analysis of concrete, which consists of two

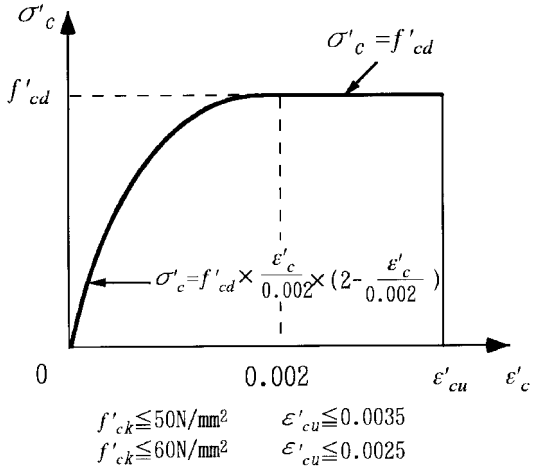

Fig. 7 Uni-axial stress-strain relation of concrete by JSCE

main loading loops, namely: the load increment loop and the load decrement loop. Within the load increment loop, the incremental elasto-plastic analysis at Step 1 and the crack analysis at Step 2 are carried out, where Δu is the displacement increment, $\Delta\varepsilon$ is the strain increment, $\Delta\sigma$ is the stress increment, and D_{ep} is the elasto-plastic matrix. These analyses go through several iterations to eliminate the residual forces of Step 3 until the solution converges at the given load. Repeat the above process until cracks initiate. After calculating the dissipation of fracture energy ΔW_f at Step 4, enter the load decrement loop to obtain the new equilibrium position *B* shown in Fig. 9. Here again, the incremental elasto-plastic analysis at Step 5 is performed, and the residual forces of Step 6 are eliminated through iterations until the solution converges. At Step 7 the strain energy loss ΔU_f is evaluated and compared with the dissipation of fracture energy ΔW_f. If the equilibrium condition $\Delta U_f = \Delta W_f$ is not yet satisfied, then continue the next round of load decrement calculations. This process is repeated until the new equilibrium position *B* is finally reached. Repetitive computations of the above two loading loops eventually lead to the failure load of the structure.

The special numerical algorithm shown in Fig. 9 now needs clarification. In the incremental elasto-plastic analysis, the total displacement is recalculated for each load increment as

$$^{i+1}u^{(1)} = {}^{i+1}u^{(0)} + ({}^{i}u - {}^{i}u^{(0)}) \tag{25}$$

with

$$^{i}u^{(0)} = {}^{i}K_0 \cdot {}^{i}P \tag{26}$$

$$^{i+1}u^{(0)} = {}^{i+1}K_0 \cdot {}^{i+1}P. \tag{27}$$

Here, $^{i+1}u^{(1)}$ is the initial displacement approximation for the present load ^{i+1}P, ^{i}u is the converged solution at the previous load ^{i}P, $^{i}u^{(0)}$ and $^{i+1}u^{(0)}$ are the reference displacements at the respective load levels. Note that the initial stiffnesses $^{i}K_0$ and $^{i+1}K_0$ are not constant; they are modified through the apparent elasticity E' whenever cracks develop. Thus, the gradual weakening of the structural stiffness and relocation of the nodal points in the vicinity of the fractured elements are monitored in the reference displacements $^{i}u^{(0)}$ and $^{i+1}u^{(0)}$. The following displacement increment

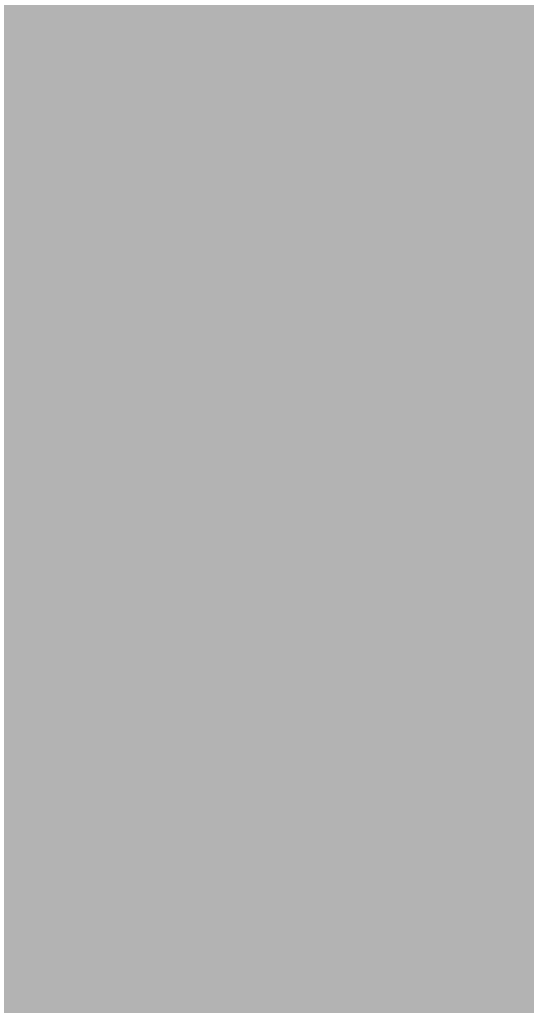

Fig. 8 Solution structure for non-linear analysis of concrete

$$\Delta u = {}^{i+1}u^{(1)} - {}^{i}u = {}^{i+1}u^{(0)} - {}^{i}u^{(0)} \tag{28}$$

is used during the first iteration to modify the predictor ${}^{i+1}u^{(1)}$, and the remaining iterations follow the Newton-Raphson procedure to eliminate the residual forces until the solution converges to ${}^{i+1}u$. Obviously, this numerical algorithm satisfies the preconditions for both the crack analysis and the incremental elasto-plastic analysis. In the iterative solutions of numerical problems, as long as a predictor is reasonable the convergence of the numerical solution can eventually be achieved through iterations by using the Newton-Raphson method.

Although no mention of the modified load control method has been made so far, it has been incorporated in the solution structure already. The modified load control method is applied when a load increment loop ends with newly extended cracks during the previous iterations. As shown in Fig. 9, the solution at this stage corresponds to Point A on the load-deflection curve, and to Point 1 in Fig. 2 of the modified load control method. In the subsequent load decrement loops, small

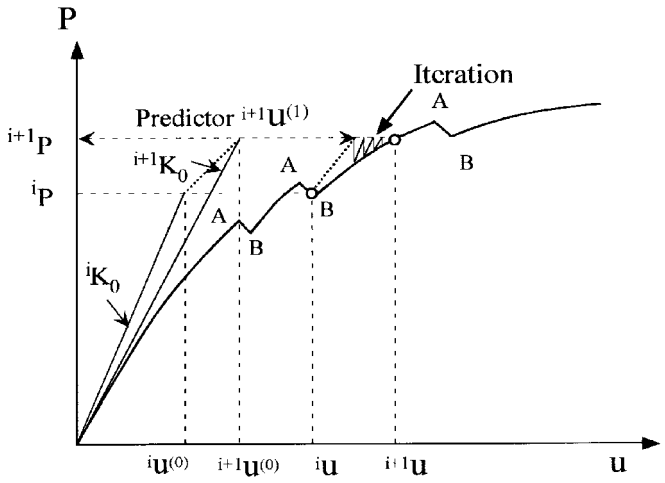

Fig. 9 Scheme for solution under load control

negative load increments are used with the newly modified initial stiffness K_0 as K^{II} in Fig. 2 to calculate the displacement decrement, and Eq. (20) serves as the criterion to terminate this guided unloading process.

This numerical model has two apparent advantages. First, the non-linear analysis is carried out using only the load control methods. Second, the crack analysis does not result in premature divergence of the numerical solutions. The effectiveness of the model has been verified extensively with experiments and reported elsewhere (Haibara *et al.* 1997, Shi and Nakano 1998, Saitoh *et al.* 1998, Osako *et al.* 1999, Yokoyama *et al.* 1999).

5. Cracking behavior of RC cantilever decks

5.1 Objective of the numerical studies

As illustrated in Fig. 1, an RC cantilever deck consists of a slab-column system where loads are transferred from the slab to the supporting column through flexure, torsion, and shear. A slab-beam system is placed between two adjacent cantilever decks. Due to its structural characteristics, hair cracks sometimes occur on the tension side of the structure, i.e., on the surface of the RC cantilever deck. In a certain sense this is unavoidable, and most building code requirements on reinforcement distribution should lead to adequate crack control. There have been actual cases, however, where the presence of only the gravity loads has led to persistent excessive cracking of the cantilever decks of wider lateral spans.

In the following, the crack behaviors of RC cantilever decks of four different proportions are analyzed, using the three-dimensional crack analysis model introduced so far. The dimensions of the four structural models studied are close to those of the practical design. Based on the numerical results, the problem is studied with respect to the patterns of crack propagation, dissipation of the fracture energy, the effects on the structural integrity, and the mechanisms which cause this type of excessive cracking.

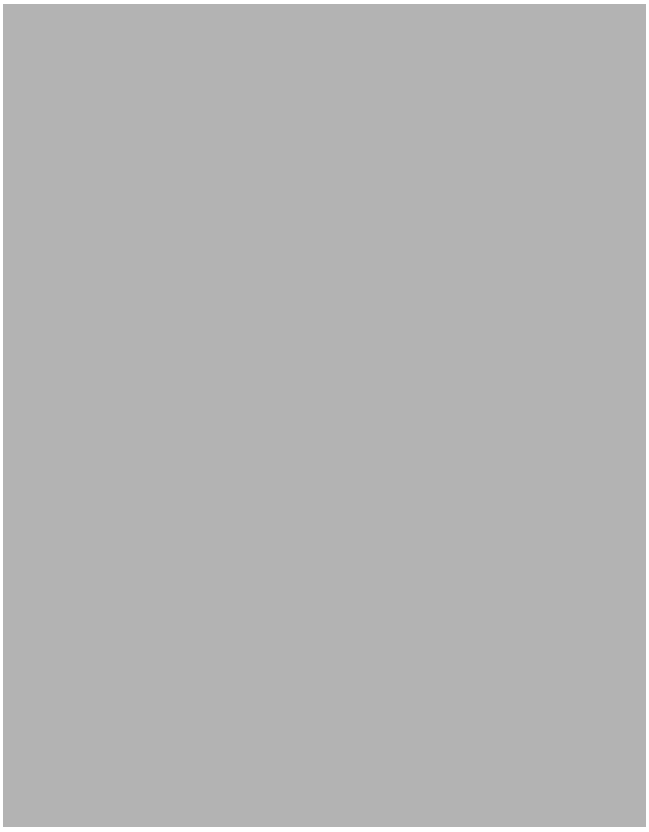

Fig. 10 Structural models for concrete and reinforcement

5.2 Outline of the numerical studies

Due to its approximate bi-axial symmetry, only a quarter of a cantilever deck is modeled to reduce the burden of numerical computations. Fig. 10 shows the four types of structural models with their reinforcement layout, where L, B and H are the lateral span, longitudinal span and depth of the deck respectively, and R is the radius of the column. The coordinates of the numerical models and the type and size of the finite element are also illustrated in the same figure. The model dimensions and material properties can be found in Table 1 and Table 2, respectively. The material properties for concrete include the elastic modulus E_c, Poisson's ratio v, the compressive strength f_c, the tensile strength f_t, the critical crack opening width ω_c, and the strain limit ε_u. For reinforcement, these are the elastic modulus E_s and the yield strength σ_y. As shown in Table 1, the width of the lateral span L varies from 6 m to 12 m while the remaining dimensions are kept constant.

Now define the span ratio as the ratio between the width of the lateral span L and longitudinal span B. The span ratios for the present study are 1.2, 1.6, 2.0 and 2.4. As far as cracking is concerned, the span ratio L/B is a critical structural parameter. Based on the numerical results of the crack analysis, the four structural models are divided naturally into two groups: the small span ratios of 1.2 and 1.6, and the large span ratios of 2.0 and 2.4. As shown later, these two groups exhibit completely different types of cracking behavior.

Table 1 Dimensions of structural models

Case	Width L (m)	Length B (m)	Depth H (m)	Radius R (m)	Span ratio L/B
1	6.0	5.0	1.5	1.5	1.2
2	8.0	5.0	1.5	1.5	1.6
3	10.0	5.0	1.5	1.5	2.0
4	12.0	5.0	1.5	1.5	2.4

Table 2 Material properties

Concrete						Reinforcing steel	
Ec (GPa)	v	f_c (MPa)	f_t (MPa)	ω_c (mm)	ε_u	E_s (GPa)	σ_y (MPa)
24.5	0.2	24.5	2.45	0.1	0.0035	205.9	353.0

The load conditions are as follows. The dead load of the cantilever deck is added at the beginning of each calculation. One fourth of the dead load of a 20 m long slab-beam system is applied incrementally along the edge of the lateral span, as shown in Fig. 10. For the boundary conditions, the nodal points on the bottom surface of a deck which are within the column radius are fixed. For the reinforcement, a simple layout of the reinforcing steel is used to replace the complicated reinforcement details in the actual design, and the reinforcement ratios for tension and compression are assumed equal. To study the restraining effect of reinforcement on cracking, two types of reinforcement ratios are assumed: ρ = 0.03, 0.06, where ρ is defined simply as the ratio of the reinforcement (in tension or in compression) area to the respective cross-sectional area of the cantilever deck. Although a more realistic modeling of the reinforcement details can be achieved using finer meshes, it is believed that even with the present degree of simplification the fundamental aspects of excessive cracking in RC cantilever decks can be properly studied.

5.3 Results and discussions

Under the dead loads, cracks appear in the top layers of the RC cantilever decks for all the cases studied. Penetration of cracks from the surface reaches up to 15 cm deep. The patterns of crack propagation and stress distributions are shown in Figs. 11 and 12 respectively.

Two completely different types of crack propagation are observed in Fig. 11. For the two cases with small span ratios, small cracks occur close to the transverse edge of the RC cantilever deck. On the other hand, for the two cases with large span ratios, large continuous cracks develop in a zone along the longitudinal central line of the deck. To clarify these differences, dissipation of the fracture energy and the effects on the structural stiffness are investigated.

5.4 Small span ratios of 1.2 and 1.6

The deck's flexural stiffnesses in the lateral (X) direction are found to be quite close to, though slightly lower than, those in the longitudinal (Y) direction. As shown in Fig. 11, cracks develop along the transverse edge, initiating almost simultaneously at the middle of the deck and at the far

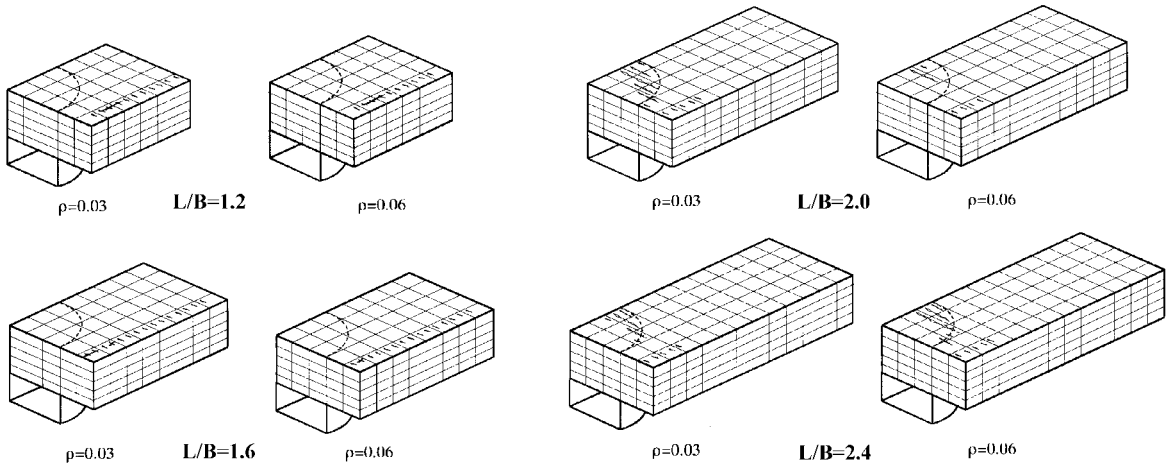

Fig. 11 Crack propagation due to dead load

end. Obviously, the occurrence of small, nearly parallel cracks in the longitudinal direction is mainly due to the weaker flexural stiffness in the transverse direction. It is interesting to find that a number of crosswise cracks develop close to the middle of the lateral span to form several two-direction cracks. As is known, two-direction cracks are quite common for equally reinforced two-way slab systems. Regarding the patterns of crack propagation, there are no significant differences between these two cases of small span ratios. The stress states under the total dead load are shown in Fig. 12. As expected, the maximum tensile stresses in the X and Y directions are very close when ρ = 0.03, and they are approximately equal as the reinforcement ratio increases to ρ = 0.06.

Fig. 13 shows the relation of the dissipated fracture energy versus the dead load. Note that both terms are divided by their respective maximum values and expressed either as a ratio or percentage. The nearly linear relation between the dissipated fracture energy and load reflects the stable nature of crack growth when the span ratios are small. The mechanism for the steady propagation of cracks is simple. As schematically illustrated in Fig. 15(a), the onset of a crack in the narrow tension zone along the transverse edge does not precipitate significant stress increases in the other parts of the zone; most of the released stresses are spontaneously transferred outside this tension area. In other words, the crack propagation is stable because the driving force for the next potential crack does not increase with the onset of the previous cracks.

A relative flexural stiffness K' defined by the ratio of the applied load to the average deflection along the transverse edge is computed and plotted against load in Fig. 14, where K_0' represents the stiffness before cracking. A conspicuous rise of the stiffness at the early stage of loading is found in the case of L/B=1.2. This is thought to be the result of the interaction between the cracked concrete and the reinforcement. A similar situation can be found in the case of L/B=1.6. It is noteworthy that as the span ratios are small, the structural stiffnesses essentially remain intact under the total dead loads. This is an important characteristic of this type of stable cracking.

Reinforcement plays an important role in regulating crack behavior. In the case of L/B=1.6, removing the reinforcing steel from the structural model completely alters the way cracks propagate. As with large span ratios to be discussed next, several large continuous cracks are found to develop in the longitudinal direction, close to the middle of the deck, before leading the structure to failure.

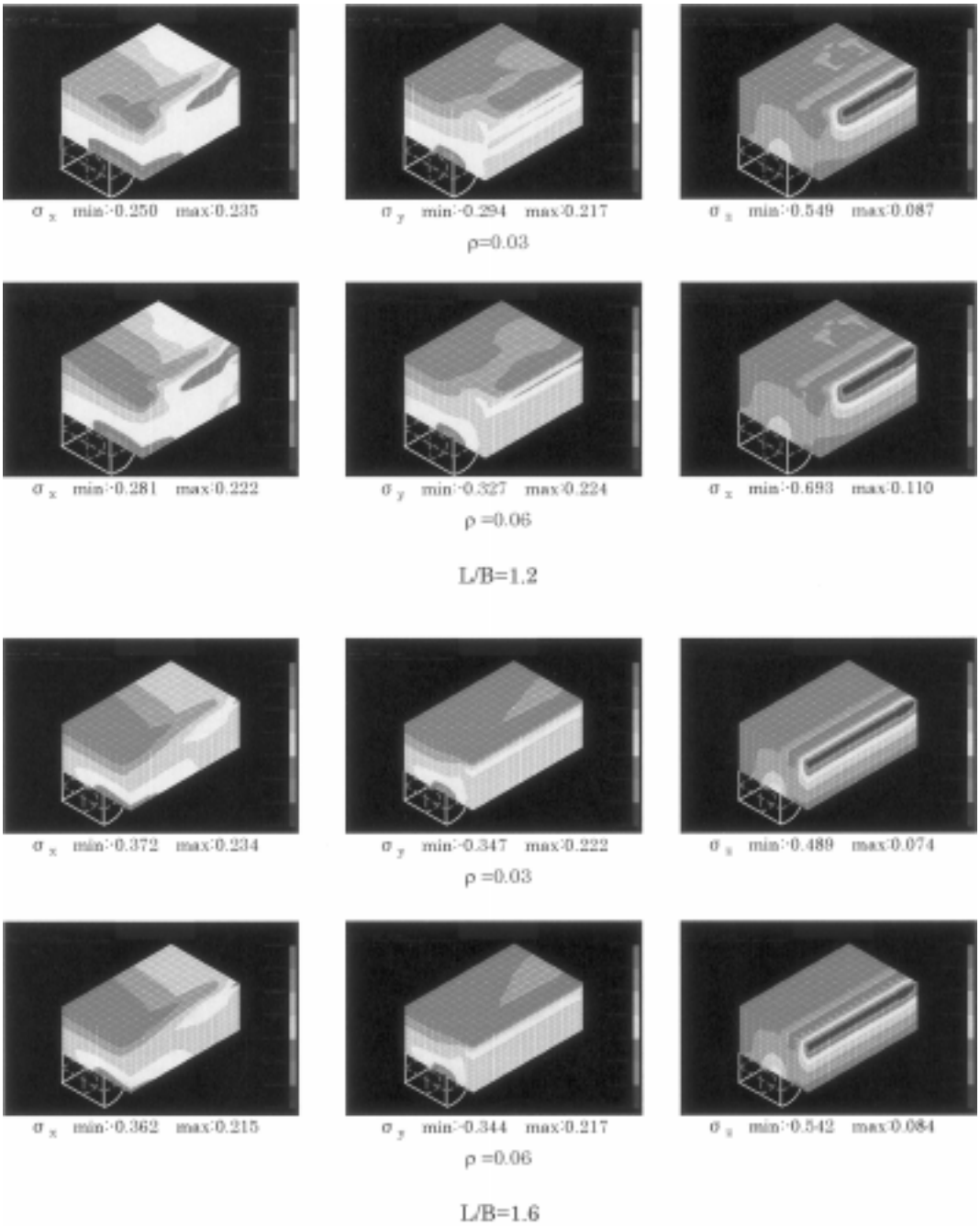

Fig. 12 Stress distributions due to dead load

5.5 Large span ratios of 2.0 and 2.4

As the span ratios increase, the deck's flexural stiffness in the transverse direction decreases significantly. As a result of this, cracks are confined to the longitudinal central zones as shown in Fig.

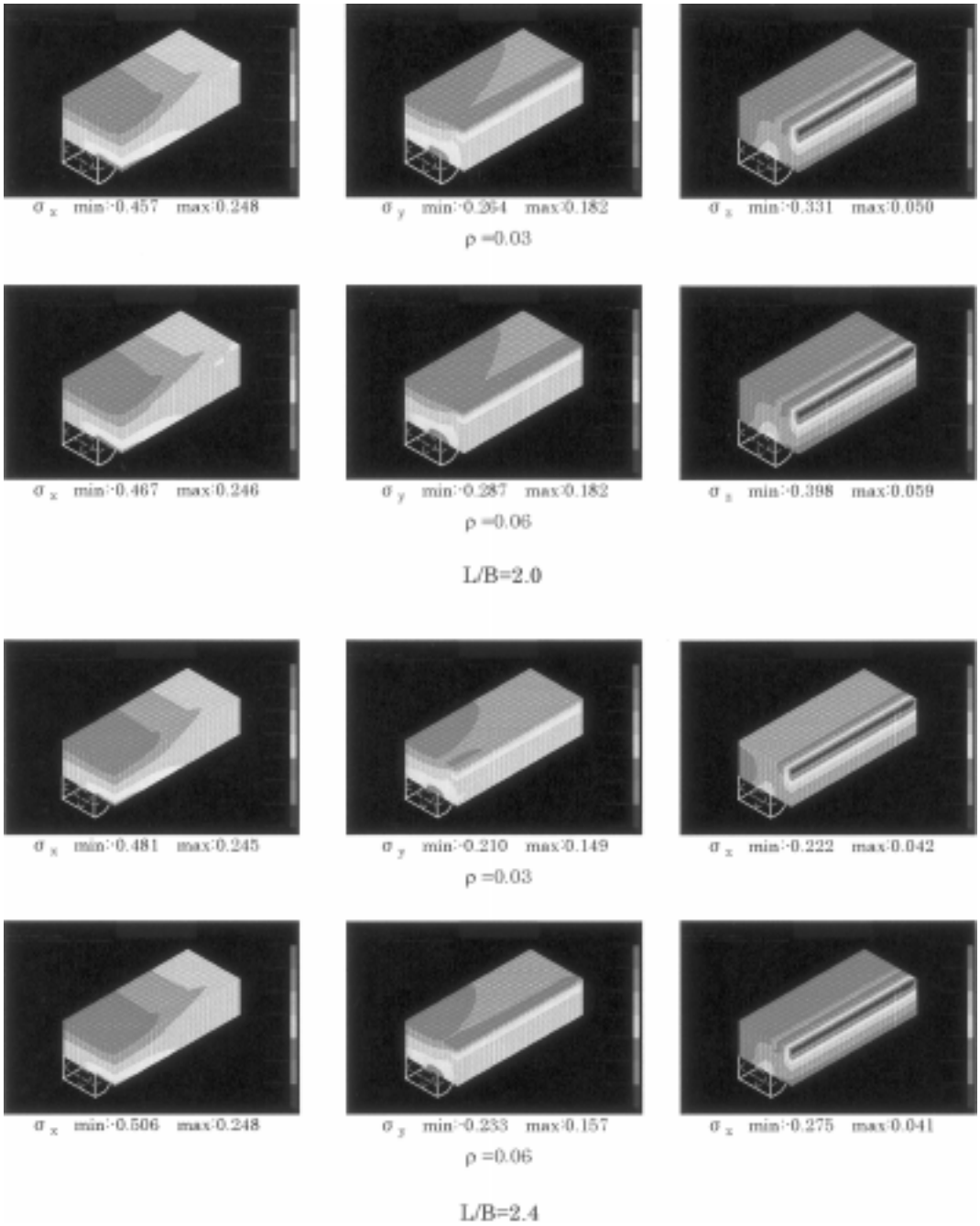

Fig. 12 Stress distributions due to dead load (Continued)

11. The width of the zone roughly equals the diameter of the supporting column. Unlike the previous cases with small span ratios, cracks initiate not only at the transverse edge, but also at the middle of the short span. After that, longitudinal cracks propagate rapidly towards the free edge to form several large parallel cracks. Crosswise cracks do not occur under the dead load, and the crack

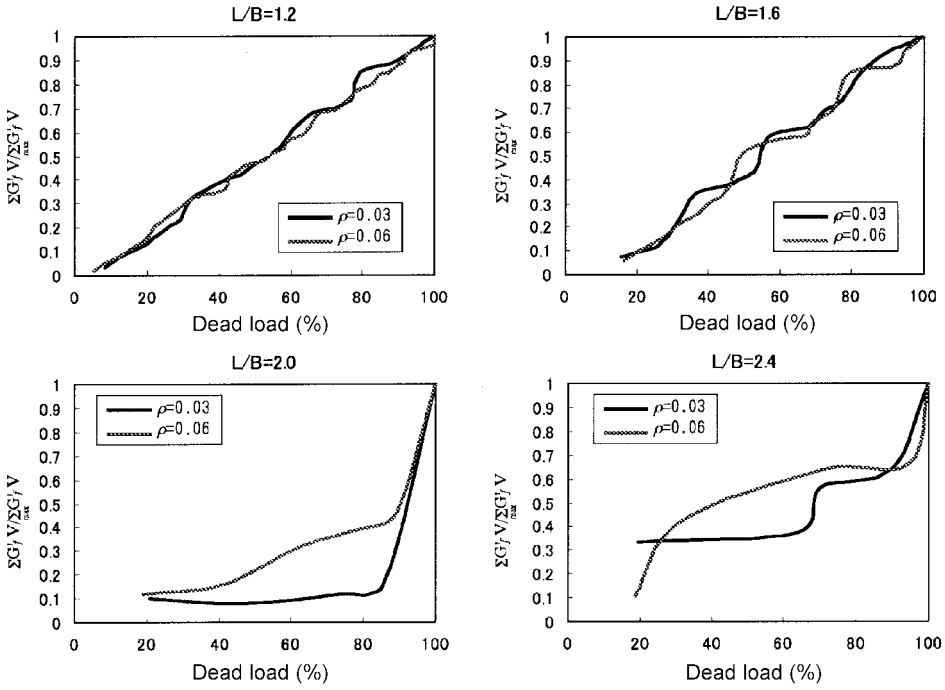

Fig. 13 Dissipated fracture energy – dead load relation

patterns are essentially the same, having little to do with reinforcement. The stress distributions in Fig. 12 reveal that the maximum tensile stresses in the Y direction are only about two thirds of those in the X direction.

In contrast to the small span ratio cases, the relation between the dissipated fracture energy and load is highly non-linear, as clearly shown in Fig. 13. As is evident from these numerical results, the crack propagation is rapid and often accompanied by a large amount of energy release, especially as the load approaches the total dead load. This type of unstable cracking can be explained using Fig. 15(b). Unlike the previous cases, the occurrence of a crack inside the present tension zone does contribute to significant stress increases in the other parts of the zone, simply because the released stress can not be transferred outside this tension area. Thus, the crack propagation becomes unstable as the driving force for fracture increases.

As shown in Fig. 14, the relative flexural stiffness monotonically decreases under the dead load, and this trend intensifies as the span ratio increases. Clearly, this exposes the harmful effects of the large continuous cracks associated with large span ratios on the structural integrity.

Last, it should be pointed out that with large span ratios, the reinforcement does not change the pattern of crack propagation to a more stable type as found with small span ratios. A further increase of the reinforcement ratio may cause the change. From the structural point of view, however, it is more efficient to change the structural type (such as using two supporting columns instead of a single column) than simply increasing the amount of reinforcement to reduce the tensile stress of concrete.

Fig. 14 Flexural stiffness – dead load relation

Fig. 15 Mechanisms of stable and unstable crack propagation

6. Summary

This paper contained two parts. In the first part the theoretical aspects of a 3-D crack analysis model were discussed. The second part focused on the application of the model to the problem of excessive cracking of RC cantilever decks.

In the first part, a modified load control method was proposed, which enabled the non-linear

response with limit points to be analyzed using only the load control methods. Next, a fracture energy approach to the crack analysis of concrete was explained. It included an energy criterion for determining the equivalent length, and an analysis method based on the variation of the fracture energy and the strain energy. Based on this approach, a three-dimensional model for crack analysis was established. One of the main features of the model is that the constitutive relations for the fractured elements are formulated based on the E'-ω relation, in order to facilitate convergence of the numerical solutions. The effectiveness of the model has been verified extensively with various fracture tests.

The extensive cracking of RC cantilever decks was investigated, with small and large span ratios. Under the given load conditions, it was found that there are essentially two types of cracking, and the crack behaviors depend very much on the span ratio. With small span ratios the crack growth is stable, and causes no apparent damage on the part of the structure. With large span ratios, however, the crack propagation is unstable due to the occurrence of large continuous cracks, which may affect the structural integrity.

References

Dahlblom, O., and Ottosen, N.S. (1990), "Smeared crack analysis using generalized fictitious crack model", *J. Eng. Mech.*, ASCE, **116**(1), 55-76.

Haibara, T., Nakatsui, K., Ito, M., and Nakatsubo, Y. (1997), "Evaluation of load carrying capacity of aging RC sewers", *Proc. the 52th Annual Conference of JSCE*.

Jones, R.M. (1975), *Mechanics of Composite Materials*, Kogakusha Ltd., McGraw-Hill.

Osako, K., Takahashi, H., Kitahashi, N., Akimoto, E., Nakatsui, K., and Nakano, M. (1999), "Renovation technology and evaluation of load carrying capacity for sewage pipe renewal method", *Proc. Int. Conf. on Infrastructure Regeneration and Rehabilitation*, Sheffield, Britain.

Saitoh, H., Kitayama, Y., and Yamashiro, H. (1998), "A new technique for sewer rehabilitation applicable to noncircular cross-sections", *Proc. the World Tunnel Congress '98 on Tunnels and Metropolises*, Sao Paulo, Brazil.

Shi, Z., and Nakano, M. (1998), "Numerical approach based on the energy criterion in fracture analysis of concrete structures", *Proc. FRAMCOS-3*, AEDIFICATIO, Germany.

Shi, Z., and Nakano, M. (1999), "Three-dimensional finite element analysis on crack behaviors of RC cantilever decks", *Construction and Building Materials*, **13**(1-2), 33-47.

Yokoyama, H., Osako, K., Koiwa, S., Kitahashi, N., and Akimoto, E. (1998), "Development of self-profiling SPR technology", *16th Int. NO-DIG '98 Poster Presentation*, CHSTT, Switzerland.